Immune evasion in primary central nervous system lymphoma: macrophage and T cell roles in response to immunotherapy

Carlota Pagès-Geli,[1-4] Daniel Medina-Gil,[1,2] Patricia Fernández-Guzmán,[1,2] Cristina Hernández,[1,2] Júlia Caràbia,[1,2] Gemma Pujadas,[1,2] Kipp Weiskopf,[3-5] Francesc Bosch[1,2,6] and Marta Crespo[1,2]

[1]Experimental Hematology, Vall d'Hebron Institute of Oncology (VHIO), Vall d'Hebron University Hospital Campus, Barcelona, Spain; [2]Department of Medicine, Universitat Autònoma de Barcelona, Bellaterra, Spain; [3]Department of Medicine, Beth Israel Deaconess Medical Center, Boston, MA, USA; [4]Harvard Medical School, Boston, MA, USA; [5]Department of Medical Oncology, Dana-Farber Cancer Institute, Boston, MA, USA and [6]Department of Hematology, Vall d'Hebron University Hospital, Barcelona, Spain

Correspondence: M. Crespo
macrespo@vhio.net

Received: November 5, 2025.
Accepted: April 16, 2026.
Early view: April 23, 2026.

https://doi.org/10.3324/haematol.2025.300015

©2026 Ferrata Storti Foundation
Published under a CC BY-NC license

Abstract

Primary central nervous system (CNS) lymphoma is an aggressive extranodal lymphoma with poor prognosis, largely due to its capacity for immune evasion within the unique microenvironment of the CNS. Here, we investigated the interactions between macrophages and T cells in a syngeneic mouse model of primary central nervous system lymphoma (PCNSL), manipulating macrophage/microglia populations and MHC class I expression on tumor cells to mimic patient-associated immune escape. We found that macrophages and microglia are indispensable for anti-tumor immunity and significantly enhance the efficacy of PD1 checkpoint blockade, particularly when tumor cells retain MHC-I expression. In contrast, depletion of these myeloid cells led to accelerated disease progression and diminished response to immunotherapy, highlighting the importance of both innate and adaptive immunity in PCNSL. Interestingly, MHC-I-deficient PCNSL did not respond to T-cell-based therapies and was controlled exclusively by macrophages, rendering prognosis largely dependent on this alteration. Our findings support the need for therapeutic strategies that target both T-cell and myeloid compartments and suggest that profiling MHC-I expression may help guide personalized immunotherapy approaches in this challenging disease.

Introduction

Primary central nervous system lymphoma (PCNSL) is a rare and aggressive form of diffuse large B-cell lymphoma (DLBCL) confined to the central nervous system (CNS), affecting the brain, spinal cord, leptomeninges, and/or eyes. It accounts for 4% of primary CNS tumors and 4-6% of extranodal lymphomas, with a median age at diagnosis of 67 years.[1] A high-dose methotrexate-based regimen followed by autologous stem cell transplantation is typically administered to fit patients, whereas whole-brain radiotherapy is often reserved for unfit patients. Despite these efforts, prognosis remains poor, with a median survival of 36 months, a 5-year survival rate of 30%, and relapse occurring in 15-25% of cases, highlighting the urgent need for new therapies.[2]

Primary central nervous system lymphoma belongs to the new term introduced in WHO-HAEM5 of primary large B-cell lymphomas of immune-privileged sites.[3] Shared features include the activated B-cell (ABC) subtype and frequent mutations in *MYD88* and *CD79B*, as well as additional genetic alterations promoting immune evasion, which are hallmarks of the MCD/C5/MYD88 genetic subtype of DLBCL.[4,5] The brain is considered an immune-privileged organ due to the limited immune surveillance and unique microenvironment, which play a crucial role in the pathogenesis and progression of the disease.[6] Moreover, up to 70% of patients exhibit tumor genetic alterations involving deletion in the *HLA* locus (6p21) and loss of *B2M* (15q21.2), which leads to reduced MHC class I (MHC-I) surface expression.[7,8] These alterations contribute to low tumor antigen presentation and T-cell recognition, preventing an efficient T-cell-mediated anti-tumoral immune response.[8] Additionally, copy-number gain of *CD274/PD-L1* (9p24.1) drives PD-L1 overexpression, which, together with MHC-I loss on lymphoma cells, enables immune evasion and is linked to poor clinical outcomes in PCNSL patients.[9-11] Given these immune checkpoint and antigen presentation defects, PD1 inhibitors like nivolumab

have been explored in the clinic.[12] However, a phase II trial reported low response rates (overall response rate: approx. 20-30%),[13] highlighting the need for further investigation.

Macrophages represent the predominant immune cells infiltrating PCNSL,[14-17] and their abundance within the tumor microenvironment (TME) is associated with a favorable prognosis.[16-18] While the PD1/PD-L1 pathway has traditionally been considered a checkpoint regulating cytotoxic responses of activated T cells,[19,20] recent studies have shown that tumor-associated macrophages (TAM) can also express PD1, and its inhibition enhances their cytotoxic activity against malignant cells.[21] Additionally, MHC-I molecules on tumor cells can bind to LILRB1 on macrophages, delivering inhibitory signals that suppress phagocytosis.[22] For that reason, downregulation of MHC-I allows lymphoma cells to evade T-cell recognition and cytotoxicity but simultaneously makes them more vulnerable to macrophage-mediated phagocytosis, particularly when inhibitory signals such as CD47 are effectively targeted.[22] Interestingly, macrophage immune checkpoints are strongly expressed in the tumor microenvironment of PCNSL patients.[14,23] Furthermore, our previous research using a patient-derived xenograft (PDX) preclinical model of PCNSL revealed high expression levels of both PD1 and SIRPα in tumoral infiltrating-macrophages.[24] This evidence highlights the strong interaction between malignant cells and macrophages in the brain, and suggests that macrophages could serve as potent effector immune cells against PCNSL lacking MHC-I expression.

Here, we assessed the infiltration and interaction of macrophages and T cells within the immune-evasive TME under immune checkpoint blockade. We achieved this using a PCNSL syngeneic mouse model by depleting macrophages and microglia, while simultaneously impairing cytotoxic T-cell function through downregulation of MHC-I on malignant B cells. This intracerebral A20 implantation represents a robust preclinical model to study immunotherapies and tumor microenvironment in PCNSL, as demonstrated by others.[24-26]

Methods

Cell lines

The murine B-cell lymphoma A20 cell line was obtained from ATCC and cultured in RPMI (ThermoFisher) supplemented with 10% FBS (ThermoFisher), 100 units/mL penicillin, 100 μg/mL streptomycin, and 292 μg/mL L-glutamine (ThermoFisher), and maintained in humidified incubators at 37ºC with 5% CO_2. For stable luciferase expression, A20 cells were transfected with a luciferase-expressing vector (Fluc2 gene).

MHC-I downregulation

CRISPR-Cas9 was performed to generate downregulation of MHC-I expression in A20 cells (MHC-I KO A20) by disrupting *TAP1*. *TAP1* gRNA, Cas9 endonuclease, and universal tracrRNA were obtained from Integrated DNA Technologies (IDT). The crRNA:tracrRNA complex was assembled following the manufacturer's protocol and delivered by electroporation using the Neon™ Transfection System (ThermoFisher).[27]

Macrophage/microglia depletion in mice

To achieve microglia depletion, mice were fed a chow diet supplemented with the CSF1R inhibitor pexidartinib (PLX3397, 290 mg/kg) for 21 days prior to intracerebral tumor implantation and maintained on this diet until endpoint. Systemic macrophages were depleted by intraperitoneal injections of clodronate liposomes at 50 mg/kg, administered daily for three consecutive days starting three days before tumor implantation, followed by twice-weekly maintenance dosing. Control groups received unsupplemented chow or PBS-containing liposomes.

In vivo modeling of primary central nervous system lymphoma

All experiments with animals were approved by the local Ethical Committee for the Use of Experimental Animals. Briefly, brains of 8-week-old BALB/c female mice were injected with 10^5 A20 cells expressing luciferase and tumor growth was monitored by bioluminescence imaging (BLI) using IVIS® Spectrum system and Living Image software (PerkinElmer).

Organ processing

Brains were collected in cold RPMI-1640 medium immediately after euthanasia. The two hemispheres were then separated with a razor blade. One hemisphere was dedicated to immunohistochemistry (IHC), while the other was processed for flow cytometry and RNA sequencing (RNA-seq). Single-cell suspensions from brains were obtained using the Tissue Neural Dissociation Kit (Papain) (Miltenyi Biotec) following the manufacturer's protocol.[28]

Flow cytometry

Cells were incubated with 1 μg IgG from rat serum (Sigma-Aldrich) per $1x10^6$ cells for 15 minutes at 4ºC, followed by staining with monoclonal antibodies for 20 minutes at 4°C. Cells were acquired in a Navios™ cytometer (BeckmanCoulter) and data were analyzed using FlowJo software (version 10.10).

Immunohistochemistry

Antigen retrieval, staining and counterstaining were performed at an Autostainer Link 48 (DAKO). Slides were scanned using NanoZoomer 2.0 HT digital slide scanner C9600 and visualized using NDP.view 2 (Hamamatsu Photonics K.K).

Multiplexed immunofluorescence and imaging analysis

Multiplex immunofluorescence (mIF) was performed on

FFPE mouse brain sections using the Opal™ Multiplex IHC Assay (Akoya Biosciences). Slides from wild-type (WT) and MHC-I knockout (KO) mice (immunocompetent [IC] and macrophage-depleted [MD] PCNSL; not treated and PD1-treated; day 15 post implantation) were stained with a panel of purified rabbit anti-mouse antibodies (CD20, CD4, CD8, TMEM119, CD68, CD86, PD1, PD-L1, CD47). Fluorescent imaging was acquired on the Vectra Polaris™ system and analyzed in QuPath. Cell-cell interactions were defined as distances of 0.5-10 μm between segmented cells.

RNA sequencing

Total RNA was isolated from mice brains following tissue dissociation. RNA quantification was performed with Qubit™ RNA High Sensitivity kit (Invitrogen) in a Qubit™ fluorometer (Invitrogen). Samples were run on NovaSeq 6000 (Illumina) with a read length of 2x50bp paired end.

Statistical analysis

The statistically significant differences between groups were assessed using the Mann-Whitney test or one or two-way ANOVA. $P<0.05$ was considered statistically significant. Survival curves were generated using the Kaplan-Meier method and statistically compared using the log-rank test. Analyses were performed using GraphPad Prism 6 software.
Additional details of the methods used can be found in the *Online Supplementary Appendix*.

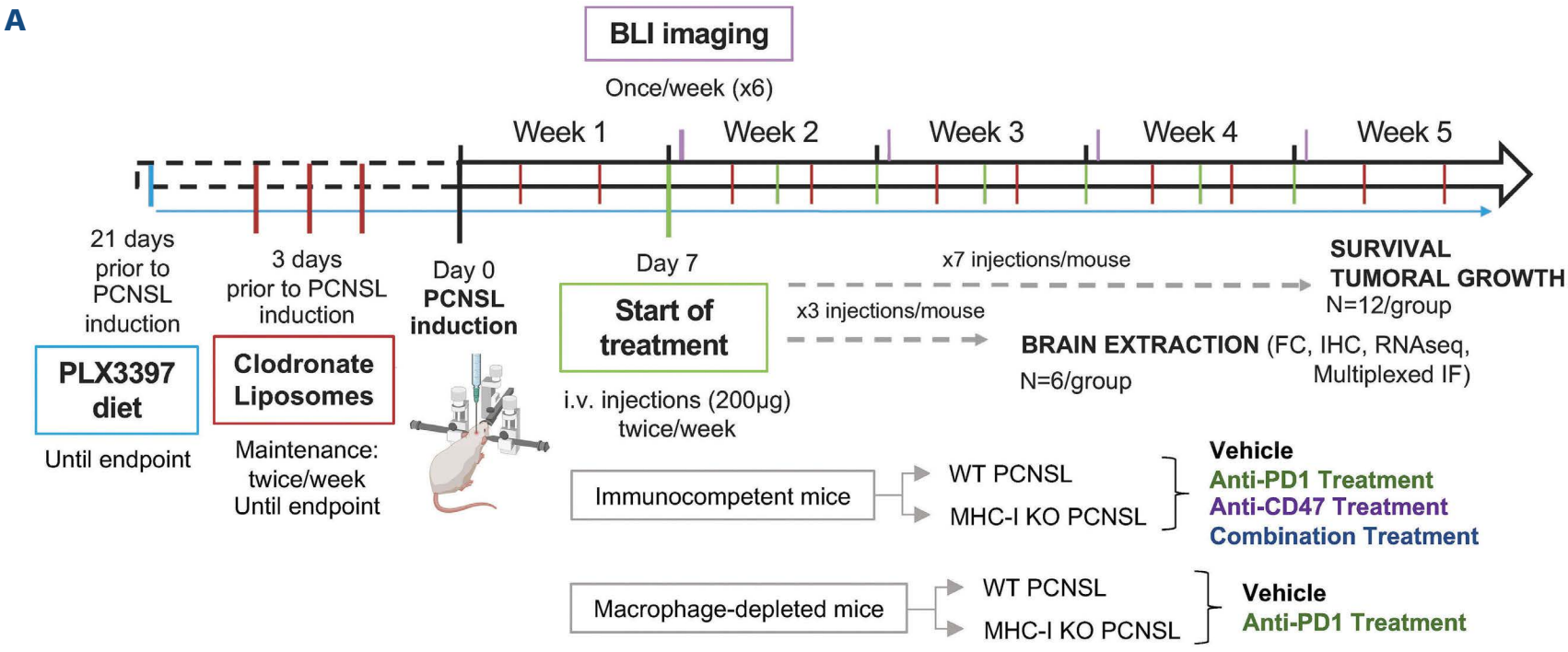
Results

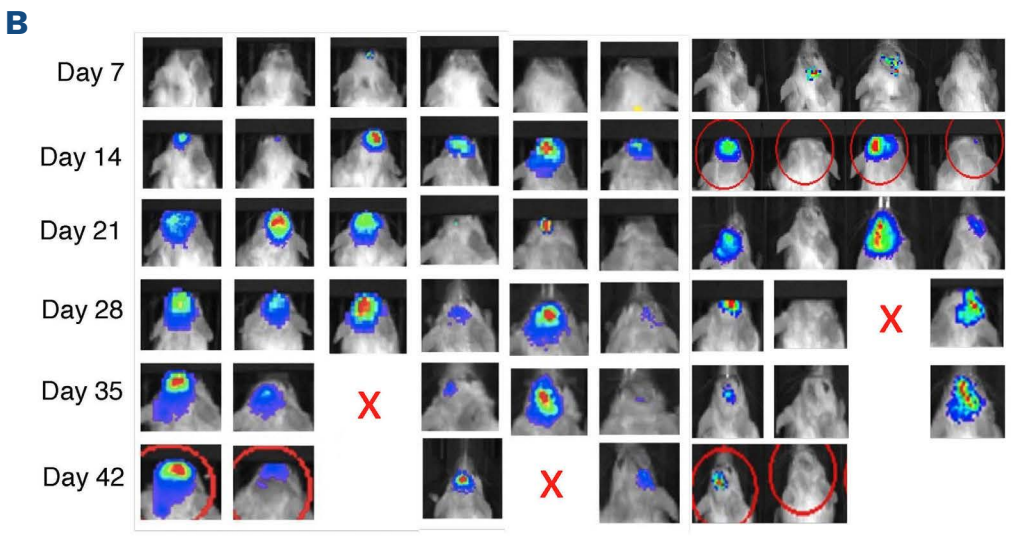
In vivo primary central nervous system lymphoma modeling

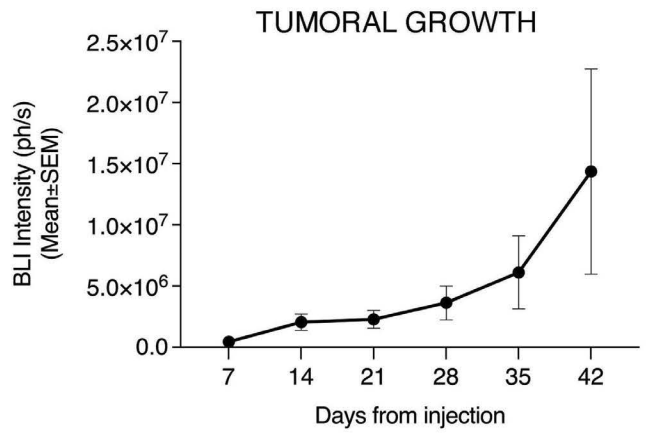
The detailed longitudinal timeline of the experimental procedure is presented in Figure 1A. To investigate the role of macrophages and MHC-I expression in PCNSL, we induced the disease in IC and MD 8-week-old BALB/c mice by intracerebrally injecting $1x10^5$ luciferase-expressing WT or MHC-I KO mature B-cell lymphoma A20 cells.[25] Survival, tumoral growth, and immune cell characterization in the brain were assessed. In all models, tumor growth was monitored twice a week starting on day 7 post-tumor injection, with a total of six captures.
In our set up model, IC mice bearing WT PCNSL had a median survival of 45 days. Tumors were already detectable in some mice seven days after brain injection (Figure 1B). At endpoint, anti-CD20 IHC revealed multifocal tumor infiltrates affecting both cerebral hemispheres, predominantly the right hemisphere, with localization primarily in the brain parenchyma where lymphoma cells formed dense clusters. In some cases, the meningeal compartment was also involved (Figure 1C).
Intravenous treatment with anti-PD1, anti-CD47 or the combination of both was initiated seven days following the intracranial injection of tumor cells, with a dosage of 200 μg in 100 μL, administered twice per week. For survival experiments, mice received a total of seven injections (N=12 mice/group). Euthanasia was performed upon reaching humane endpoints, including weight loss, circling behavior, motor impairments, and increased head size. To investigate immune infiltration in the brain, the same groups were studied, and brains were harvested 15 days post-tumor inoculation (N=6 mice/group), following the administration of three treatment injections.
To study the role of macrophages in PCNSL, both systemic macrophages and brain microglia were depleted. IHC staining for Iba-1 demonstrated complete depletion of systemic macrophages in the spleen and liver after three consecutive daily injections of clodronate liposomes prior to tumor induction (Figure 2A). Maintenance injections were given at the same concentration twice/week after tumor inoculation. In the same manner, partial microglia reduction in brain was achieved by continuously exposing mice to a pexidartinib diet for ten days, with complete depletion reached by day 21 (Figure 2B). At this point, PCNSL tumors were established with continuous exposure to a pexidartinib diet until endpoint to ensure ongoing microglia depletion. We also assessed macrophage and microglia depletion in mice bearing PCNSL following this schedule. We evaluated CD11b expression by flow cytometry. Results showed a significant reduction in both myeloid cell populations in the TME at final point (Figure 2C), with only residual staining attributable to cellular debris, indicating significant depletion of both macrophages and microglia in the tumor-bearing brain at endpoint, which confirmed sustained depletion under the subsequent maintenance regimens (*Online Supplementary Figure S1A*).
To down-regulate the surface expression of MHC-I on malignant cells, we employed CRISPR-Cas9 to target the *TAP1* gene. *TAP1* encodes a transporter involved in loading peptides onto MHC-I molecules[29] and its downregulation reduces surface MHC-I expression. Validation of the KO was performed through flow cytometry (Figure 2D) and Sanger sequencing (*Online Supplementary Figure S1B*).
Strong positive expression of PD-L1 and CD47 surface proteins in both WT and MHC-I KO A20 cells were detected by flow cytometry (*Online Supplementary Figure S1C*).

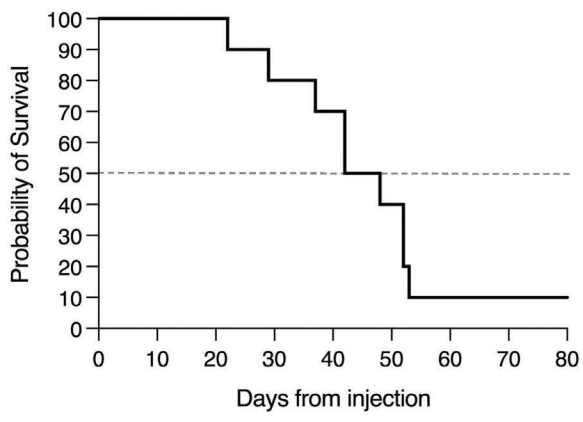
Lack of expression of MHC-I in primary central nervous system lymphoma induces a more aggressive disease and reduces overall survival

To investigate the role of MHC-I expression in PCNSL, we induced the disease in IC mice by intracerebrally injecting luciferase-expressing WT or MHC-I KO A20 cells (N=12). Tumor progression was monitored by BLI, and survival was evaluated. Mice bearing MHC-I-negative tumors exhibited a more aggressive disease, with significant differences in tumor growth apparent as early as day 7 post implantation, and continuing through later stages, compared to WT tumor growth (Figure 3A). To determine if the proliferative advan-









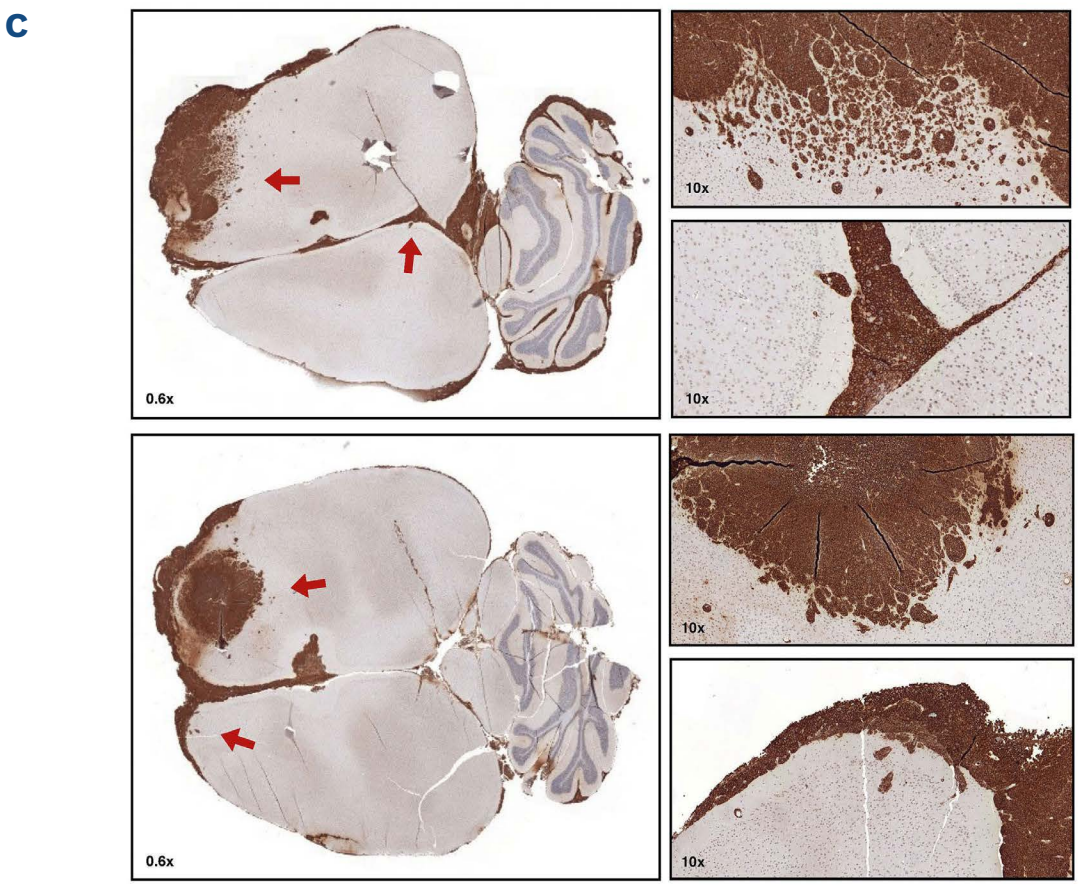


Figure 1. Primary central nervous system lymphoma *in vivo* set up. (A) Overview of the experimental design and timeline. (B) Bioluminescence imaging of mice bearing primary central nervous system lymphoma (PCNSL), captured from day 7 to day 42 post-tumor injection at 7-day intervals. Quantification of tumoral growth and survival curves are represented. (C) CD20 immunohistochemical staining of mouse brain sections with PCNSL. Presence of lymphoma cells within the brain parenchyma and meninges is indicated by red arrows. Whole-brain images are displayed at 0.6x magnification, while higher-resolution images focusing on the parenchyma and meninges are shown at 10x magnification.

tage of lymphoma cells was intrinsic to MHC-I downregulation, they were cultured *in vitro* under identical conditions; however, no significant differences in cell growth kinetics over time between WT A20 and MHC-I KO A20 cells were observed (Figure 3B). This faster-growing tumor translated into a significantly longer survival of WT tumor-bearing

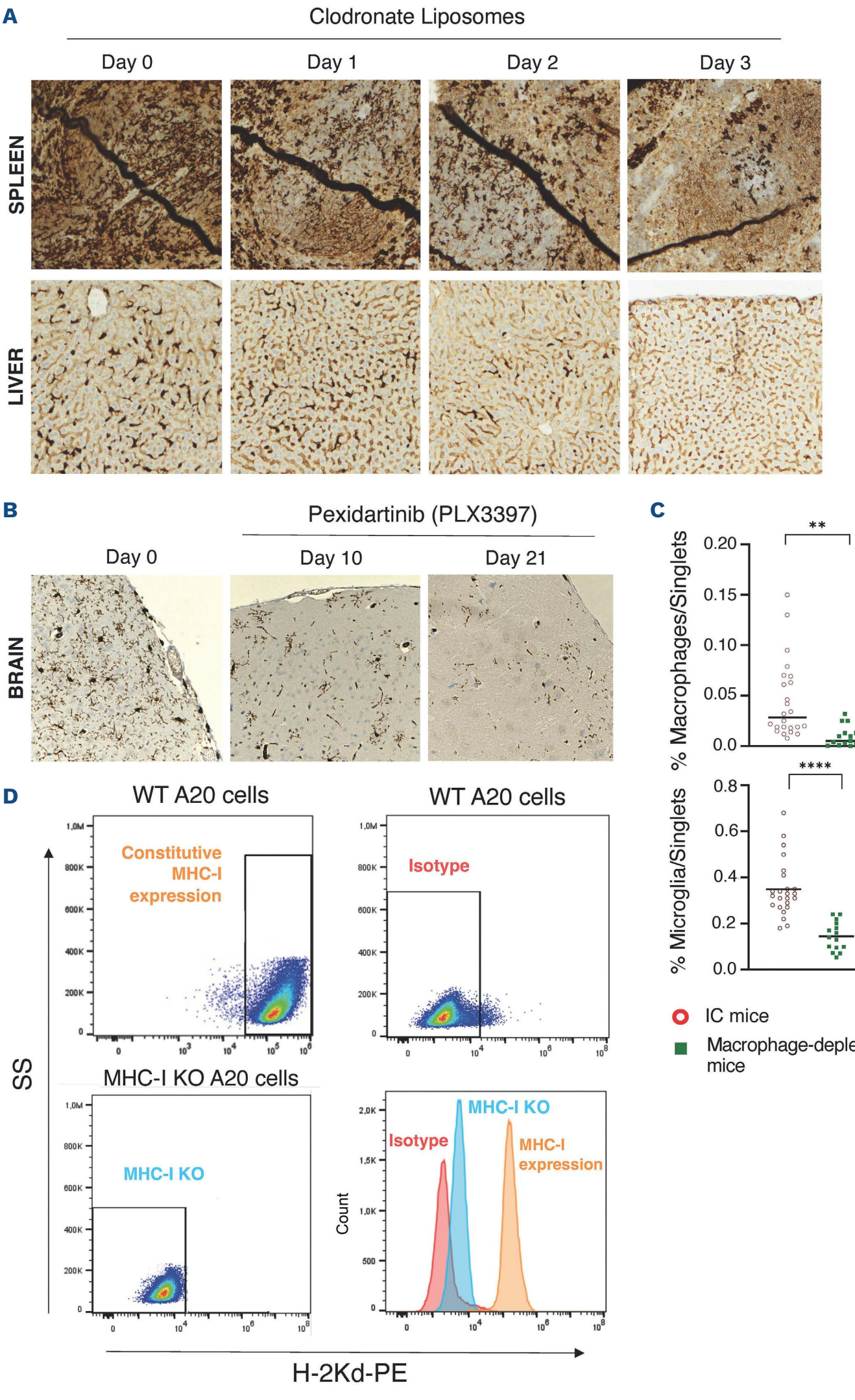
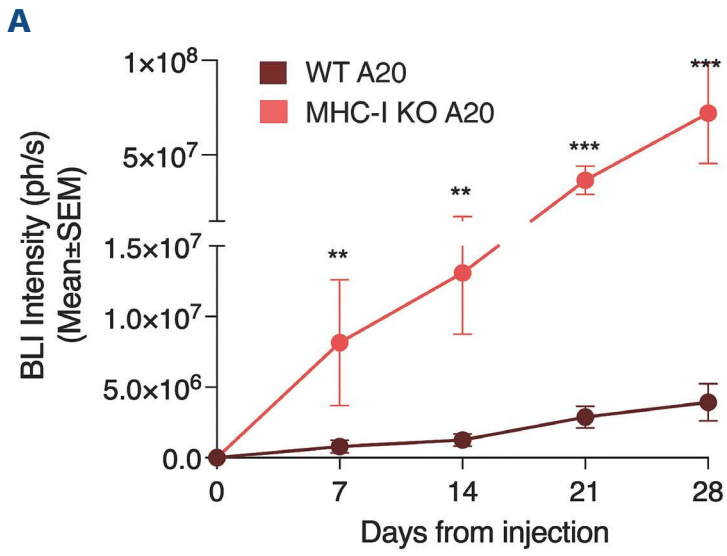
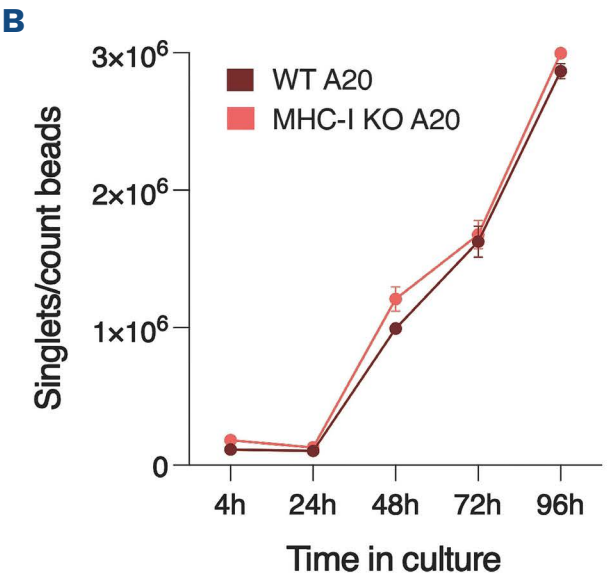
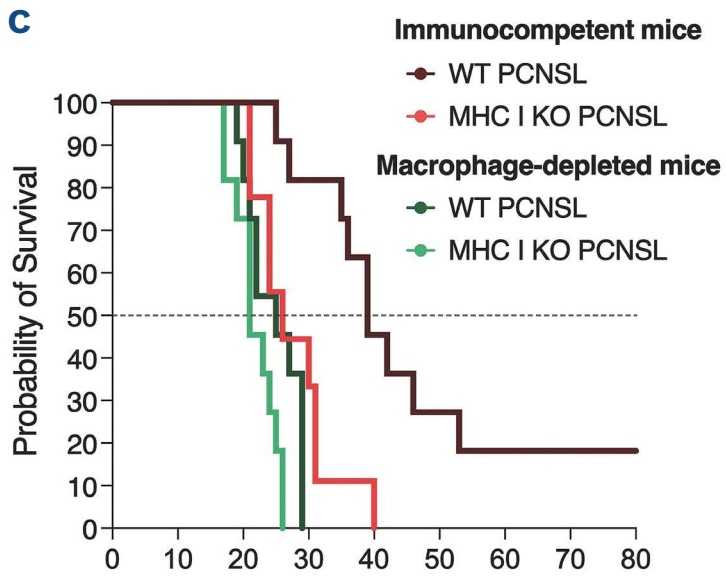
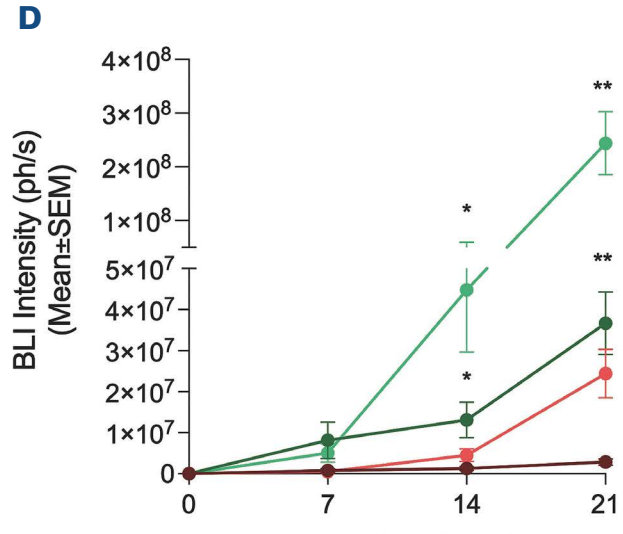


Figure 2. Macrophage/microglia depletion and MHC-I knockout set up. (A and B) Microglia and macrophage staining. Immunohistochemistry (IHC) of Iba-1-stained macrophages in FFPE spleen and liver sections from mice treated with clodronate liposomes, comparing control (day 0) and different timepoints. Images were captured at 10x magnification (A). IHC of Iba-1-stained microglia in FFPE brain sections from mice treated with the anti-CSF1R drug pexidartinib (PLX3397) at baseline (day 0), day 10, and day 21 post treatment (B). (C) Detection of $CD11b^{+}$ macrophages and microglia by flow cytometry after primary central nervous system lymphoma (PCNSL) induction. Macrophages identified as $CD45^{high}CD11b^{+}$ cells (left) and microglia identified as $CD45^{low}CD11b^{+}$ cells (right) in brain tissue. Plots show percentages of cells (out of singlets) in PCNSL-induced immunocompetent mice (red) and macrophage-depleted mice (green). Mann-Whitney test: $^{**}P<0.01$, $^{****}P<0.0001$. (D) Validation of MHC-I knockout by CRISPR-Cas9 using flow cytometry. Dot plots and histogram showing surface expression of MHC-I in A20 cells. Constitutive expression in wild-type (WT) A20 is shown, as well as expression after the CRISPR. SS:.....









IC mice	WT	12	7	2	2
	MHC-I KO	12	3	0	0
MD mice	WT	10	0	0	0
	MHC-I KO	8	0	0	0

Numbers at risk

Median survival

Immunocompetent mice		Macrophage-depleted mice	
WT PCNSL	MHC-I KO PCNSL	WT PCNSL	MHC-I KO PCNSL
39	26	25	21

** P=0.002
* P=0.01
*** P=0.0002
* P=0.04

Figure 3. Tumoral growth and survival of immunocompetent and macrophage-depleted mice bearing either wild-type or MHC-I knockout primary central nervous system lymphoma. (A) *In vivo* growth of wild-type (WT) and MHC-I knockout (KO) A20 cells in brains of immunocompetent mice. Sample size: N=12 per group. Data are presented as mean bioluminescence intensity (BLI) intensity (ph/s) ± standard error of mean (SEM). Mann-Whitney test: **P<0.01, ***P<0.001. (B) *In vitro* growth of WT and MHC-I KO A20 cells. Proliferation was assessed by counting viable cells every 24 hours (h) using flow cytometry with counting beads. Data are presented as the mean of two replicates ± SEM. Dark red represents WT cells, while light red indicates MHC-I KO cells. (C and D) Results are organized into two groups comparing immunocompetent (IC) and macrophage-depleted (MD) mice. Within each group, mice were induced with either WT primary central nervous system lymphoma (PCNSL) (dark red for IC and dark green for MD mice) or MHC-I KO PCNSL (light red for IC and light green for MD mice). Kaplan-Meier survival plot represents the probability of survival over 80 days, with median survival days indicated for each group. Numbers at risk for days 20, 40, 60 and 80 are shown. Significant differences in survival are shown by P values determined using the Log-rank test (C). Tumor growth curves are displayed as mean BLI ± SEM for each group over time until day 21. Mann-Whitney tests were conducted to compare tumor types growing in MD mice with their respective tumor types in IC mice at each timepoint; *P<0.05, **P<0.01 (D).

mice compared to MHC-I KO tumor-bearing mice (median survival: 39 days [WT, dark red line] *versus* 26 days [MHC-I KO, light red line]; Kaplan-Meier, *P*=0.002) (Figure 3C). This suggests that MHC-I-negative lymphoma cells may possess a proliferative advantage *in vivo* within the brain microenvironment, where T cells are unable to recognize them and exert a cytotoxic effect. In this context of absence of the MHC-I-LILRB1 inhibitory signaling pathway, we hypothesize that macrophages may exhibit increased antitumoral activity. However, this potential increase in macrophage activation would not be reflected in the aggressiveness of MHC-1 negative PCNSL, possibly because, unlike T cells, macrophages may require additional stimulation. Consistent with this, MHC-II deficient PCNSL exhibited comparable tumor growth and immune profiles to WT tumors *in vivo* (*Online Supplementary Figure S2*), emphasizing that MHC-I, rather than MHC-II, serves as a key determinant of immune control and a potential prognostic factor in PCNSL.

Macrophages control the tumoral growth in primary central nervous system lymphoma and prolong mice overall survival

To uncover the role of macrophages and microglia in PCNSL, we also injected WT or MHC-I KO A20 lymphoma cells into the brains of MD mice (N=12 per group) and assessed tumor growth and survival. Results demonstrated that both WT and MHC-I KO tumors exhibited a faster tumoral growth in the absence of macrophages in the tumor microenvironment compared to the same tumors growing in IC mice (Figure 3D). Accordingly, survival analysis also showed significant differences in IC compared to MD mice (Figure 3C). In MD mice, both WT (see Figure 3C: dark green line) and MHC-I KO (see Figure 3C: light green line) PCNSL had approximately the same short median survival rates (25 *vs*. 21 days; *P*=0.04), meaning that the absence of macrophages and microglia cells is sufficient to induce a very aggressive disease, even in WT tumors.

To understand the aggressiveness of MHC-I KO tumors, it is important to note that survival of mice bearing MHC-I KO PCNSL with a fully intact immune cell compartment (see Figure 3C: light red line) closely mirrored that of mice carrying WT tumors growing in the absence of macrophages and microglia (see Figure 3C: dark green line) (26 *vs*. 25 days). This suggests that macrophages and/or microglia may play a critical role in controlling the initial tumoral growth of CNS lymphoma cells in the brain and supports the observation of limited T-cell activity in MHC-I KO tumors, highlighting the necessity of stimulating the myeloid compartment to enhance an anti-tumoral immune response in this setting.

PD1-blockade immunotherapy is more effective when macrophages are present in the tumor microenvironment

The loss of MHC-I surface expression in malignant cells resulted in more aggressive disease in our syngeneic mouse model of PCNSL. Recognizing the critical role of macrophages in controlling malignant cell growth within this microenvironment, we hypothesized that anti-PD1 treatment may exert anti-tumoral effects by enhancing macrophage phagocytic activity, even in the context of MHC-I down-regulation. To investigate the roles of macrophages and T cells in the response to checkpoint inhibitors, we utilized both IC and MD mice bearing either WT or MHC-I KO PCNSL tumors. For each model, 48 mice were used and divided into two cohorts based on tumor type (WT A20 cells or MHC-I KO A20 cells; N=24 per cohort). Each cohort was then split into two treatment groups: vehicle control or anti-PD1 antibody (N=12 per group). Anti-PD1 therapy was initiated seven days after tumor induction and administered intravenously twice weekly for a total of seven doses. Results showed that in WT CNS lymphoma, significant differences in tumor growth between treated and non-treated groups became apparent starting at day 14 post-tumor injection in IC mice (see Figure 4A: dashed dark red line *vs*. solid dark red line). In contrast, in MHC-I KO CNS lymphoma, no significant differences in tumor growth were observed between anti-PD1-treated mice and the vehicle group at any timepoint, although a modest response to treatment was noted (see Figure 4A: dashed light red line *vs*. solid light red line).

To evaluate the specific role of macrophages in the therapeutic activity of PD1 blockade, we compared vehicle-treated and anti-PD1 treatment groups in MD mice. No significant differences were observed between control and anti-PD1 treatment in any group, indicating that a robust anti-PD1 treatment response is achieved when macrophages are present in the TME (Figure 4B). In terms of survival, PD1 blockade significantly prolonged survival in IC mice bearing both WT PCNSL (see Figure 4C: dashed dark red line *vs*. solid dark red line; unreached *vs*. 39 days; *P*=0.0005) and MHC-I KO PCNSL (see Figure 4C: dashed light red line *vs*. solid light red line 43.5 *vs*. 26 days; *P*=0.0002) (Figure 4C). Notably, the survival of IC mice with MHC-I KO tumors treated with anti-PD1 was comparable to that of non-treated mice bearing WT tumors (dashed light red line *vs*. solid dark red line; 43.5 *vs*. 39 days). Interestingly, in the absence of macrophages and microglia, only those bearing WT PCNSL tumors had a significant survival advantage from treatment (see Figure 4D: dashed dark green line *vs*. solid dark green line; 50 *vs*. 25 days; *P*=0.005). MHC-I KO tumor-bearing mice did not respond to anti-PD1 treatment in MD mice (see Figure 4D: dashed light green line *vs*. solid light green line; 19 *vs*. 21 days) (Figure 4D).

Overall, anti-PD1 treatment is less effective in the absence of macrophages and microglia in both genetic scenarios, suggesting myeloid cells actively participate in the anti-tumoral response to the treatment in PCNSL. We confirm that MHC-I-negative CNS lymphomas can only be controlled by

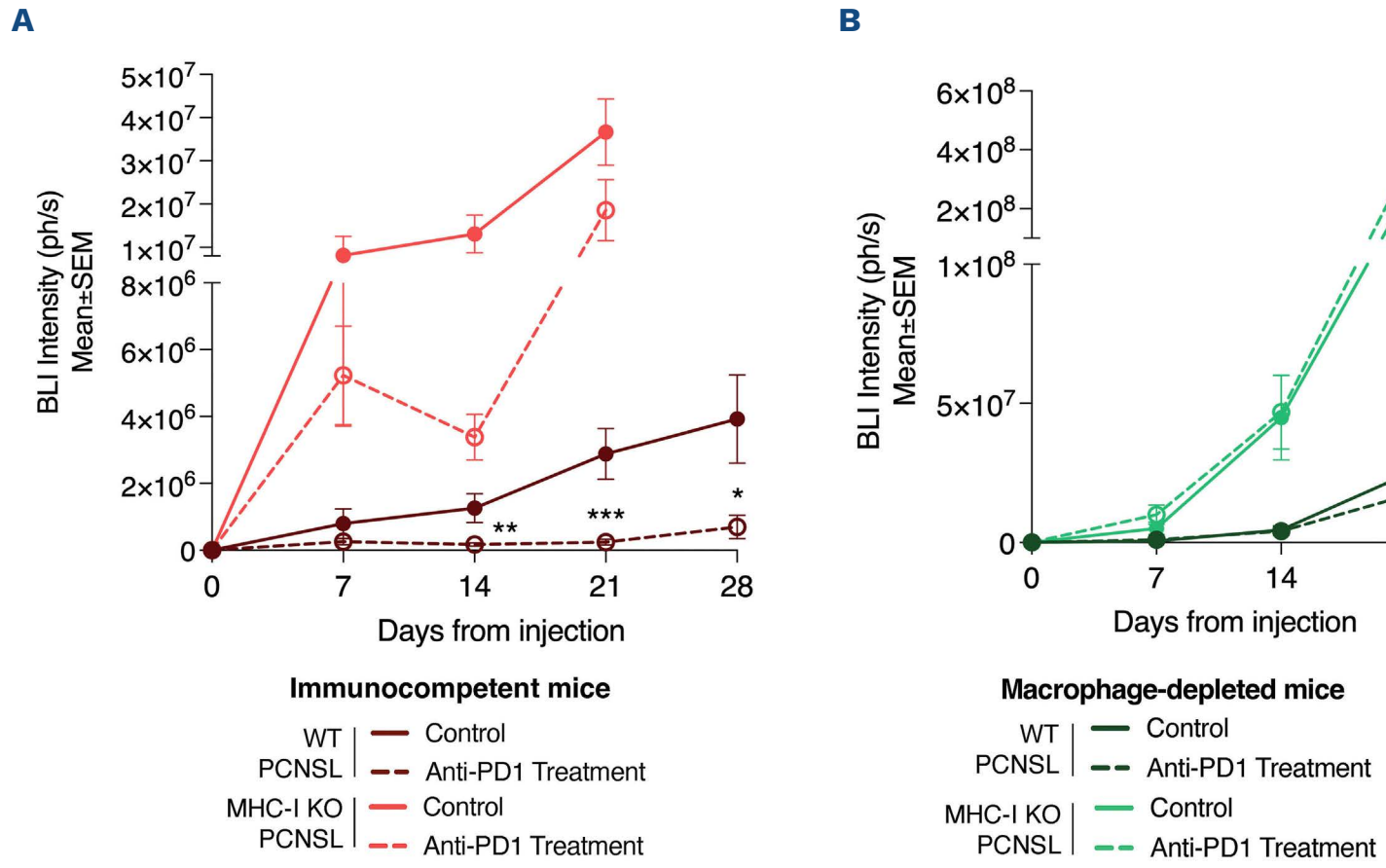


Figure 4. Effect of anti-PD1 treatment on tumoral growth and survival in primary central nervous system lymphoma mouse models. (A and B) Tumoral growth in mice bearing primary central nervous system lymphoma (PCNSL) treated with anti-PD1. Tumor growth curves are shown for each group over time, up to day 21 or 28 (until last timepoint with all mice alive), in immunocompetent mice (A) and macrophage-depleted mice (B), bearing either wild-type (WT) or MHC-I knockout (KO) PCNSL. Solid

Continued on following page.

lines represent non-treated groups, while dashed lines represent groups treated with anti-PD1. Sample size: N=12 mice/group. Data are presented as mean bioluminescence intensity ± standard error of mean. The legend provides color-coded lines for the different groups. (C and D) Kaplan-Meier survival curves of mice bearing PCNSL. Survival plots illustrating the probability of survival over 80 days for immunocompetent mice (C) and macrophage-depleted mice (D), bearing either WT or MHC-I KO PCNSL. Median survival days for each group are indicated below the curves. Solid lines represent non-treated groups, while dashed lines represent groups treated with anti-PD1. Numbers at risk for days 20, 40, 60 and 80 are shown. Significant differences in survival are represented by *P* values determined using the Log-rank test. CTL: Control (Vehicle). NS: not significant.

macrophages. However, PD1 blockade alone is insufficient to reduce the aggressiveness of MHC-I KO CNS tumors, indicating that disrupting the PD1/PD-L1 interaction does not fully engage macrophages to eliminate the tumors.

Blocking the CD47- SIRPα immune checkpoint pathway is not enough to engage a complete macrophage anti-tumoral response in MHC-I negative central nervous system lymphomas

To explore immunotherapies that can further potentiate macrophage anti-tumoral activity in MHC-I-negative CNS lymphomas, we next treated mice bearing WT or MHC-I KO tumors with either anti-CD47 (targeting the key macrophage immune checkpoint CD47-SIRPα pathway) alone or in combination with anti-PD1. Interestingly, significant improvement in survival was observed only in MHC-I-negative PCNSL mice compared to controls (see Figure 5A: dashed light purple line *vs*. solid light purple line; 37 *vs*. 26 days; *P*=0.0017) (Figure 5A), suggesting that macrophages are more active against MHC-I KO tumors under CD47 blockade (*Online Supplementary Figure S3A*). However, MHC-I KO PCNSL presented generally lower responses than WT PCNSL to anti-PD1, anti-CD47 and combination treatments (*Online Supplementary Figure S3B*). We observed no synergistic effect of the combination across tumor types (Figure 5B), which we confirmed *in vitro* by co-culturing SG+(StayGold) MHC-I KO A20 cells with BALB/c-mice derived macrophages and quantifying tumor growth over seven days (*Online Supplementary Figure S3C*). Treatment with the combination showed no enhanced phagocytosis or further reduction in tumor cell growth.

Overall, these results indicate that MHC-I KO CNS lymphomas remain highly aggressive under CD47 blockade, and that this immune checkpoint inhibition is insufficient to improve outcomes in mice bearing these tumors. An important observation from these results is that macrophages respond, at least partially, to these immunotherapies, indicating their potential as effector immune cells in treating MHC-I-negative CNS lymphomas. Additional immunotherapies need to be explored to fully activate macrophage-mediated cytotoxicity against these tumors.

Macrophages and microglia drive immune suppression and modulate T-cell infiltration

To further characterize macrophages and T cells participating in the antitumor response, we harvested brains on day 15 after tumor induction and analyzed the infiltrating immune cell populations by flow cytometry, immunohistochemistry (IHC) and mIF. Our analyses revealed a significant association between the abundance of myeloid cells in the tumor microenvironment and the expression of immune checkpoints on tumor cells.

By IHC, we observed a stronger infiltration of $CD3^+$ T cells in WT PCNSL tumors compared with MHC-I KO tumors in IC mice (Figure 6A, *Online Supplementary Figure S4*). This difference was also maintained in MD tumors, although overall infiltration levels were markedly lower, confirming that macrophages are required to sustain a full T-cell infiltration and effective immune response. mIF confirmed that tumor infiltrating T cells were exclusively $CD8^+$ cytotoxic T cells, indicating that antitumor immunity in PCNSL primarily depends on MHC-I rather than MHC-II pathways.

Interestingly, expression of PD-L1 and CD47 on tumor cells was markedly reduced in the absence of macrophages and microglia (Figure 6B). This finding correlates with the diminished infiltration of $CD8^+$ T cells observed in MD tumors, indicating impaired T-cell activation compared to IC mice. In contrast, IC tumors exhibited a coordinated immune response characterized by high infiltration of $CD86^+$ macrophages and $CD8^+$ T cells in the tumor core, where interactions between immune cells (macrophages in orange and $CD8^+$ T cells in green) and tumor cells (purple) were highly evident (Figure 6C). Notably, T cells were absent from non-tumoral regions, highlighting their specific recruitment to the tumor site.

We hypothesize that myeloid cells may actively shape an "immune-hot" microenvironment, which promotes upregulation of immune checkpoints on lymphoma cells as an adaptive response to immune pressure. In a setting with intact macrophages, tumor cells expressing higher levels of PD-L1 and CD47 are likely preferentially selected, as these molecules inhibit macrophage-mediated phagocytosis and thereby protect lymphoma cells from clearance.

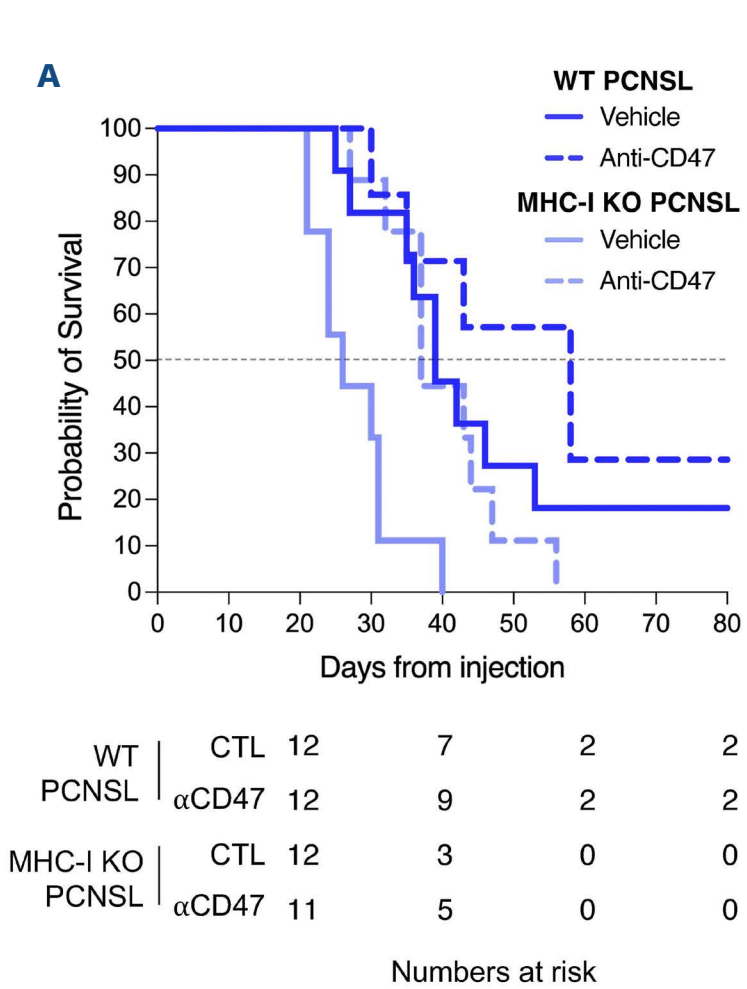
Interestingly, this pattern was reversed in the MHC-I-deficient setting, where PD-L1 and CD47 expression on lymphoma cells was reduced (Figure 6B). In this MHC-I-deficient context, we consistently observed reduced T-cell infiltration and activation (Figure 6A, C, Online *Supplementary Figure S4*), reflecting a lower adaptive antitumor immunity due to failed antigen presentation and cytotoxic T-lymphocyte priming. These data reveal that T cells, rather than macrophages alone, serve as the dominant upstream regulators of checkpoint upregulation within the lymphoma tumor microenvironment. Specifically, $CD8^+$ T cells would provide the primary IFNγ signal that transcriptionally induces PD-L1 (*via* JAK1/STAT1/

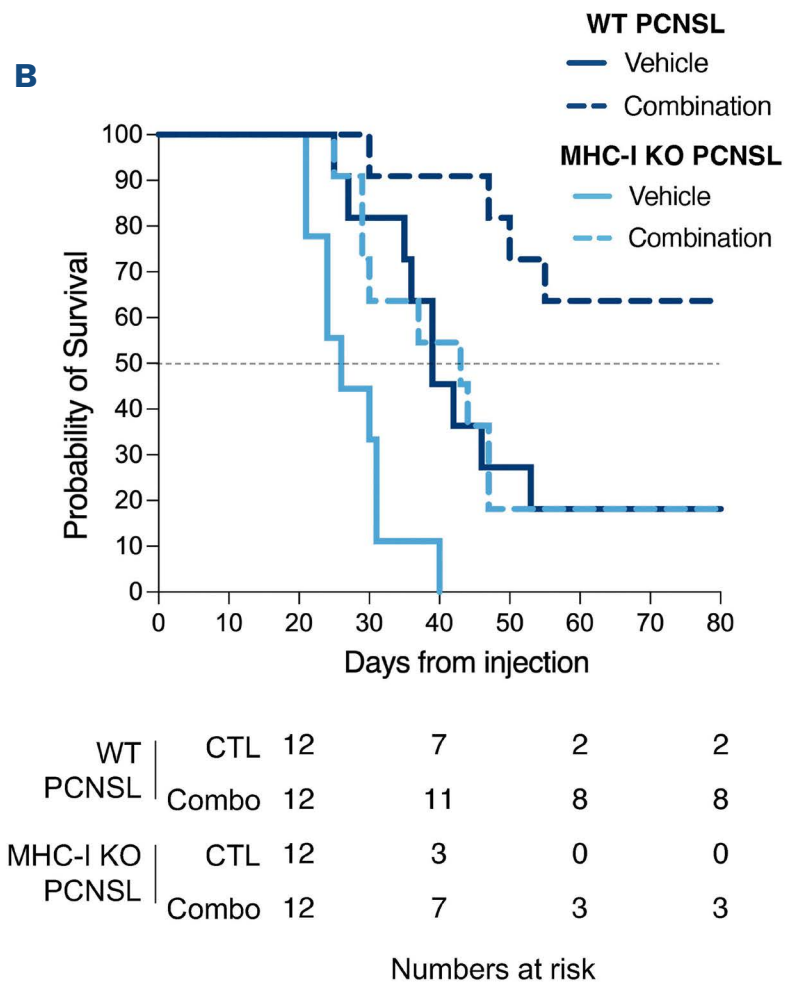
IRF1) and CD47 (through parallel STAT1 and IRF1 activation) as an adaptive resistance mechanism, creating a feed-forward loop where initial tumor recognition paradoxically amplifies immune inhibitory ligands. Macrophages would amplify this circuit secondarily via TNFα/IL-6 but cannot independently sustain it without T-cell-derived IFNγ, explaining why both MHC-I loss (eliminating T-cell activation) and macrophage depletion (removing amplification) independently attenuate checkpoint expression on lymphoma cells.

Overall, in our experiments, a robust antitumoral response was only observed when lymphoma cells expressed MHC-I, enabling effective T-cell activity that synergized with macrophage function. Conversely, loss of either T-cell-mediated recognition (through MHC-I deficiency) or macrophage activity (through cell depletion) is associated with lower immune checkpoint expression and a more aggressive tumor phenotype, highlighting that macrophages alone, in the absence of T-cell help or therapeutic intervention, are insufficient to control MHC-I-deficient lymphoma.

In the myeloid compartment, microglia were the most prevalent non-tumoral immune cells throughout the brain parenchyma, and macrophages had already infiltrated the TME by day 15. As previously demonstrated in a preclinical model of PCNSL,[24] these cells were highly concentrated in proximity to CD20$^+$ tumoral cells, suggesting a direct interaction with the tumor (Figure 6D).

Both microglial cells and macrophages (Iba1$^+$ cells) located within the tumor displayed enlarged cell bodies and more complex branching compared to those in non-tumoral regions, where Iba1 staining was weak. Such morphological activation has previously been associated with improved outcomes in CNS lymphoma patients.[16-18] To determine whether microglia





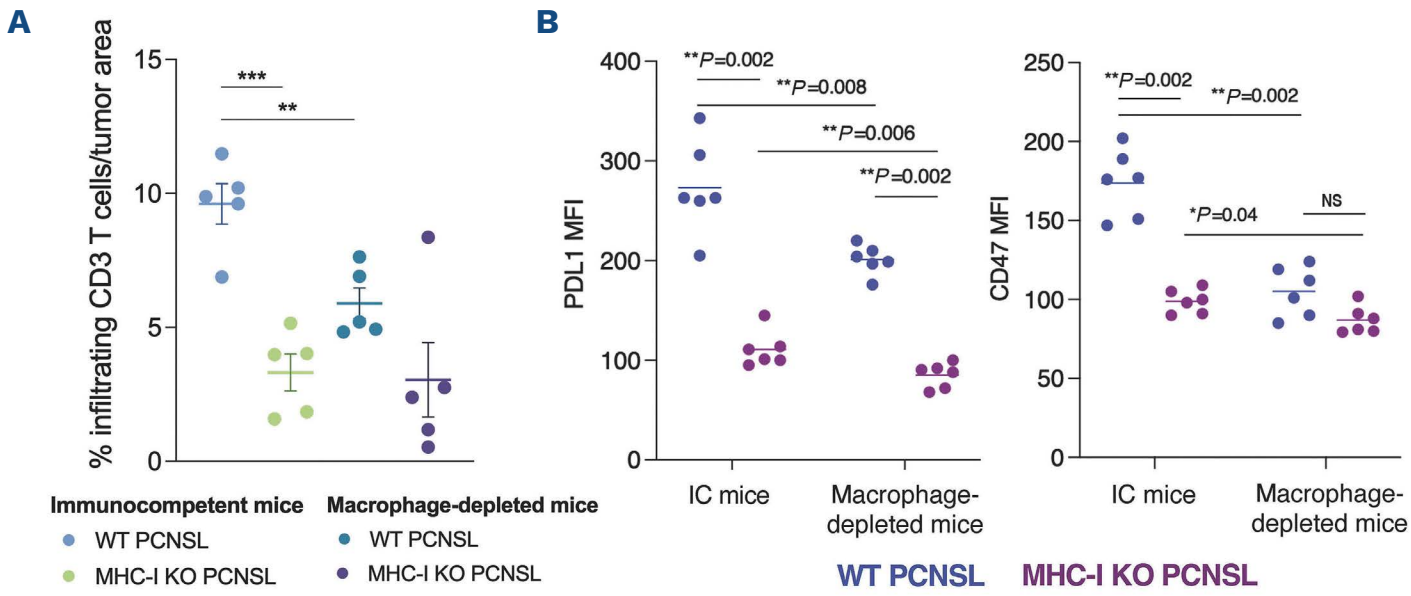
Median survival

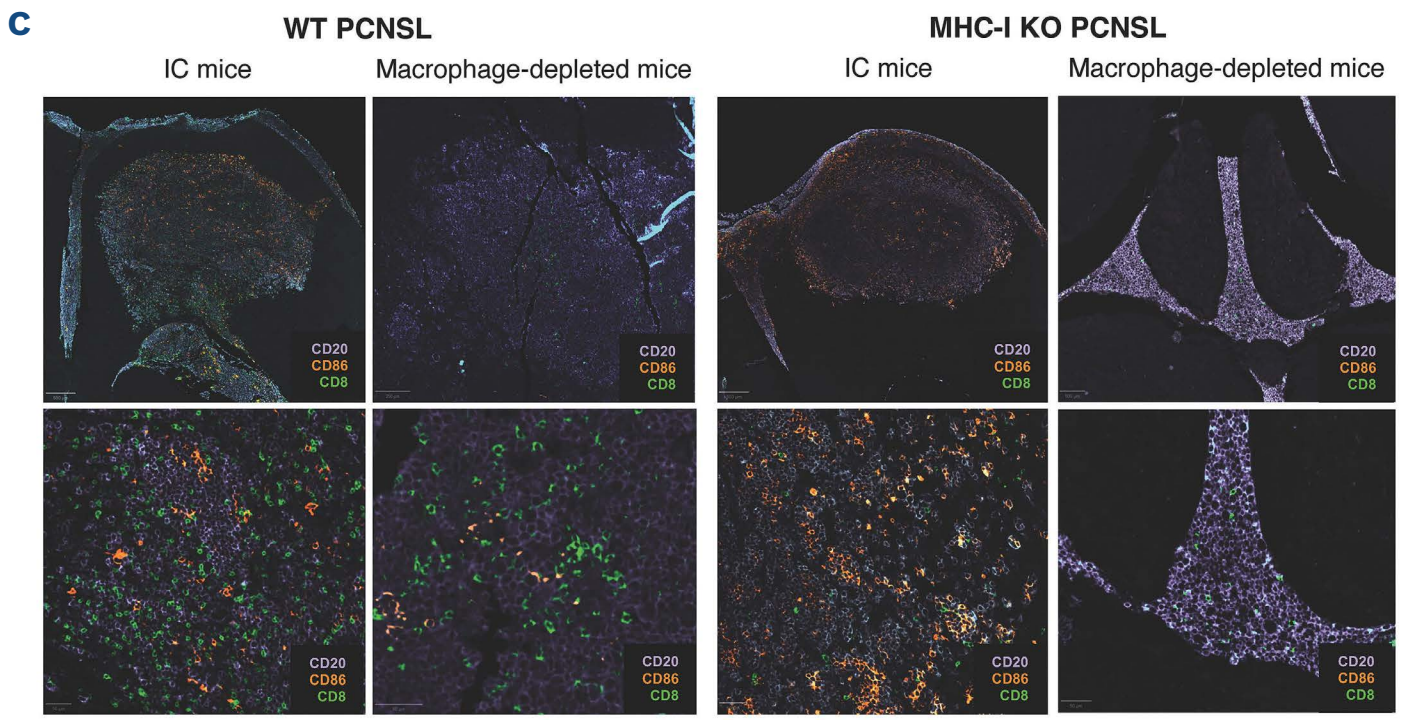
WT PCNSL		MHC-I KO PCNSL	
Vehicle	Anti-CD47	Vehicle	Anti-CD47
39	58	26	37
NS		$^{**}P$=0.0017	

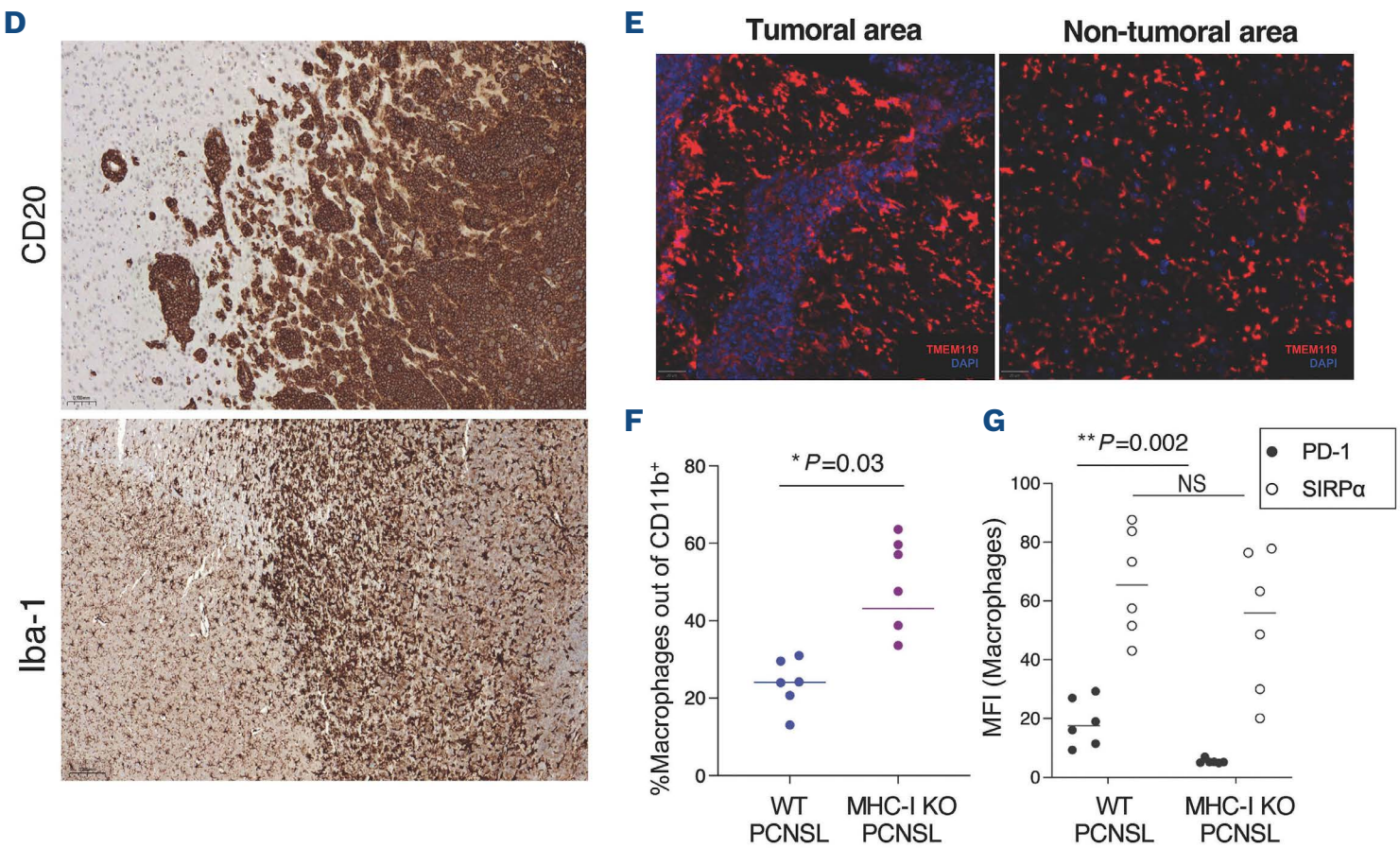
Median survival

WT PCNSL		MHC-I KO PCNSL	
Vehicle	Combo	Vehicle	Combo
39	Undefined	26	43
$^{*}P$=0.01		$^{**}P$=0.005	

Figure 5. Effect of anti-CD47 and combination treatments on survival in immunocompetent primary central nervous system lymphoma mouse models. (A and B) Kaplan-Meier survival curves of mice bearing primary central nervous system lymphoma (PCNSL). Survival plots illustrating the probability of survival over 80 days for immunocompetent (IC) mice with wild-type (WT) or MHC-I knockout (KO) PCNSL. Mice were treated with anti-CD47 treatment (A), or combination (combo) of anti-PD1 and anti-CD47 treatments (B). Median survival days for each group are indicated below the curves. Significant differences in survival are represented by *P* values determined using the Log-rank test. CTL: Control (Vehicle). NS: not significant.







Continued on following page.

Figure 6. Characterization of immune cell infiltration in mouse brains with primary central nervous system lymphoma. (A) Percentages of infiltrating CD3$^+$ T cells were quantified in the tumoral area of immunohistochemistry (IHC) slides using QuPath (number of CD3$^+$ cells / number of CD20$^+$ cellsx100). Five vehicle-treated samples per group were analyzed (N=5). Significant differences between groups were assessed using the Mann-Whitney U test. (B) Surface expression of PD-L1 and CD47 on tumor cells. Data are represented by mean fluorescence intensity (MFI). Purple represents wild-type (WT) primary central nervous system lymphoma (PCNSL), while maroon represents MHC-I knockout (KO) PCNSL. Significant differences between groups were determined using the Mann-Whitney U test, with *P* values indicated. (C) Representative images of the tumor microenvironment from multiplexed immunofluorescence (mIF) staining (rabbit anti-mouse CD20, CD86, and CD8) in vehicle-treated mouse brains. Images derive from immunocompetent and macrophage-depleted mice bearing WT or MHC-I KO PCNSL tumors. Top row: 100-500 μm scale; bottom row: 50 μm zoom-in. (D) IHC of brain tissue stained for CD20$^+$ tumor cells. The same region stained for Iba-1, showing the distribution of macrophages and microglia. High infiltration of macrophages and the increased size of both macrophages and microglia in areas with a high concentration of tumor cells is shown. Brains were extracted from immunocompetent mice bearing either WT or MHC-I KO PCNSL. 100 μm scale for CD20. (E) Representative images of TMEM119-stained tumoral and non-tumoral areas, highlighting microglia. Scale bar: 20 μm. (F) Percentage of macrophages out of CD11b$^+$ cells by flow cytometry. Purple represents WT PCNSL, while maroon represents MHC-I KO PCNSL. Significant differences between groups were determined using the Mann-Whitney test, with *P* values indicated. (G) Expression of PD1 and SIRPα, represented by MFI, in macrophages. Expression of markers was performed by flow cytometry of brain samples from WT or MHC-I KO tumor-bearing immunocompetent mice. Significant differences between groups were determined using the Mann-Whitney test, with *P* values indicated.

contribute to the antitumor response, we assessed TMEM119 expression by IF and found that these exhibited activated, enlarged morphologies, specifically when in contact with tumor cells, supporting their role in the local immune response (Figure 6E). This pattern was consistently observed across all tumor settings in which microglia were present, indicating that these resident immune cells can respond to the tumor independently of tumor type or therapeutic strategy.

The percentage of macrophages among total CD11b$^+$ cells was higher in MHC-I KO tumors, suggesting increased infiltration of these cells, potentially due to the aggressiveness of the tumor (Figure 6C, F). IF analysis revealed that most infiltrating macrophages expressed CD86, consistent with an activated phenotype. Moreover, PD1 expression in macrophages was significantly higher in WT PCNSL (Figure 6G). This suggests that higher PD-L1 expression in WT tumor cells likely leads to greater macrophage engagement through PD1, triggering increased PD1 expression on macrophages as a feedback mechanism. A slight, but not significant, decrease of SIRPα was also observed.

PD1 blockade triggers a T cell-dependent antitumor response that requires MHC-I expression in primary central nervous system lymphoma

Because the absence of an effective antitumor response in MHC-I negative tumors was not due to the absence of major immune cell subsets in the brain, we first examined PD1 expression on T cells as a marker of activation in untreated tumors. We found a significantly lower frequency of PD1$^+$ CD3$^+$ T cells within MHC I KO tumors compared to WT tumors, especially in an MD setting (Figure 7A), confirming that T-cell activation and antitumor effector function are reduced in the absence of MHC I in PCNSL. Upon anti-PD1 treatment, WT tumors exhibited a pronounced increase in T-cell infiltration within the tumoral area (Figure 7B), accompanied by a strong upregulation of PD1 on T cells and elevated PD-L1 expression on tumor and immune cells (Figure 7C, *Online Supplementary Figure S5*), consistent with an active, IFN γ–driven immune response. In contrast, this treatment-induced T-cell infiltration and immune activation were largely absent in MHC-I KO tumors, indicating that effective T-cell recognition through MHC-I is necessary to mount a productive response to checkpoint blockade. As expected, CD47 blockade failed to promote T-cell recruitment into the tumor microenvironment. Interestingly, in MD mice, anti-PD1-induced T-cell infiltration into WT tumors was maintained (Figure 7B).

Multiplex IF analysis of cellular interactions revealed that the number of close contacts between CD8$^+$ T cells and CD20$^+$ tumor cells was significantly increased in anti-PD1-treated WT tumors compared to non-treated controls (Figure 7D). Infiltration of Iba1$^+$ myeloid cells (macrophages and microglia) within the tumor microenvironment was comparable across groups in IC mice (Figure 7E). In addition, mIF revealed similar microglia distributions across samples, and elevated CD86$^+$ macrophage infiltration in MHC-I KO PCNSL tumors (Figure 6C); however, the small sample size precludes strong conclusions.

T cell-to-macrophage ratios were higher in WT PCNSL tumors, particularly under anti-PD1 treatment (Figure 7F), which indicates T-cell dominance, albeit small numbers preclude reaching significance, and is generally associated with improved prognosis in cancer.[30] This spatial organization supports enhanced T cell-tumor engagement crosstalk following PD1 blockade, further highlighting the dependence of an effective antitumor immune response on MHC-1 restricted T-cell recognition.

RNA-sequencing analysis highlights MHC-I-dependent T-cell activation and immune surveillance in primary central nervous system lymphoma

To investigate differences in gene expression, we performed RNA-seq on brains extracted from mice 15 days after tumor induction. Using supervised analysis, we compared the gene expression profiles of IC mice and MD mice. This analysis revealed significant differential gene expression between the two groups. In mice bearing WT PCNSL tumors, 1,534 genes

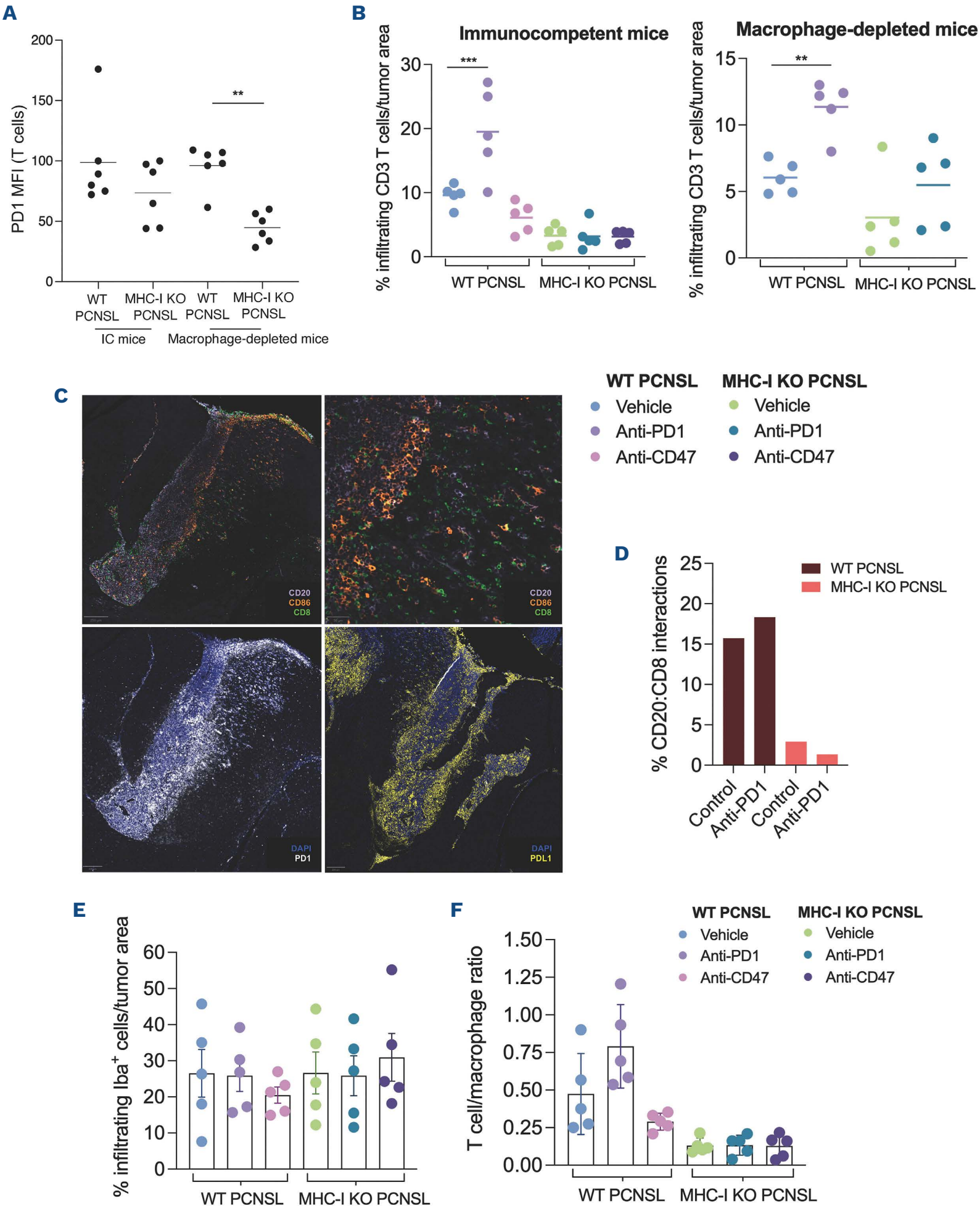


Figure 7. Effect of immune checkpoint blockade treatment in immune cell infiltration in mouse brains with primary central nervous system lymphoma. (A) Mean fluorescence intensity (MFI) expression of PD1 in T cells. Expression was checked in non-treated immunocompetent and macrophage-depleted mice bearing wild-type (WT) primary central nervous system lymphoma (PCNSL) and MHC-I knockout (KO) PCNSL. (B) Percentages of infiltrating $CD3^+$ T cells were quantified in the tumoral area of immunohistochemistry (IHC) slides using QuPath (number of $CD3^+$ cells / number of $CD20^+$ cells x 100). Samples from immunocompetent and macrophage-depleted mice bearing WT or MHC-I KO tumors (treated with vehicle, anti-PD1, or anti-CD47) were analyzed (N=5 per group). Significant differences between groups were determined using the Mann-Whitney U test. (C) Representative images of the tumor microenvironment from multiplexed immunofluorescence staining (rabbit anti-mouse CD20, CD86, and CD8

Continued on following page.

in the top row, and DAPI, PD1 and PDL1 in the bottom row) in vehicle-treated mouse brains. Images derive from immunocompetent and macrophage-depleted mice bearing WT or MHC-I KO PCNSL tumors. Top row: 50-250 μm scale; bottom row: 200 μm zoom-in. (D) Percentage of $CD20^+$ tumor cells interacting with $CD8^+$ T cells within the tumoral area in vehicle- and anti-PD1-treated mice bearing WT or MHC-I KO PCNSL. Interactions were defined as cell-cell proximity <15 μm using QuPath. (E) Percentages of infiltrating $Iba1^+$ cells quantified in the tumoral area of IHC slides using QuPath (number of $Iba1^+$ cells / number of $CD20^+$ cells x 100). Samples from immunocompetent and macrophage-depleted mice bearing WT or MHC-I KO tumors (treated with vehicle, anti-PD1, or anti-CD47) were analyzed (N=5 per group). (F) T cell/macrophage ratios were calculated as $CD3^+$/$Iba1^+$ cell numbers in the same groups as in (E).

were up-regulated and 1,284 were down-regulated in IC conditions compared to MD conditions (*Online Supplementary Table S1*). Similarly, in mice bearing MHC-I KO PCNSL tumors, 414 genes were up-regulated and 323 were down-regulated under the same comparison (*Online Supplementary Table S2*). To understand the biological roles of these differentially expressed genes, we conducted Gene Set Enrichment Analysis (GSEA) using the mouse Reactome database. In WT PCNSL tumors, we observed a significant upregulation of pathways associated with MHC-I signaling, PD1, and CD3/TCR phosphorylation in IC mice compared to their counterparts in MD mice (Figure 8A). These findings suggest that in the absence of macrophages and microglia, compensatory T-cell activation occurs, which slows tumor growth. In contrast, in MHC-I KO PCNSL tumors, the absence of T-cell activation led to significantly more aggressive tumor growth. This is driven by the upregulation of pathways associated with proliferation, mitosis, and cytokine/interleukin signaling, highlighting the critical role of immune surveillance in controlling tumor progression (Figure 8B).

We further interrogated the dataset by directly comparing the transcriptional effects of anti-PD1 treatment and MHC-I depletion. PD1 blockade led to upregulation of immune activation and interferon response-related pathways in WT PCNSL tumors, in both IC and MD mice, consistent with enhanced immune effector activity (*Online Supplementary Tables S3, S4*, *Online Supplementary Figure S5A, B*). This was not observed in MHC-I KO PCNSL tumors (*Online Supplementary Figure S5C)*. In contrast, MHC-I deficiency was associated with upregulation of DNA repair, replication stress, and chromatin remodeling pathways, indicating activation of proliferative and genome-stabilizing programs in MHC-I-deficient tumors (*Online Supplementary Table S5*, *Online Supplementary Figure S6C*).

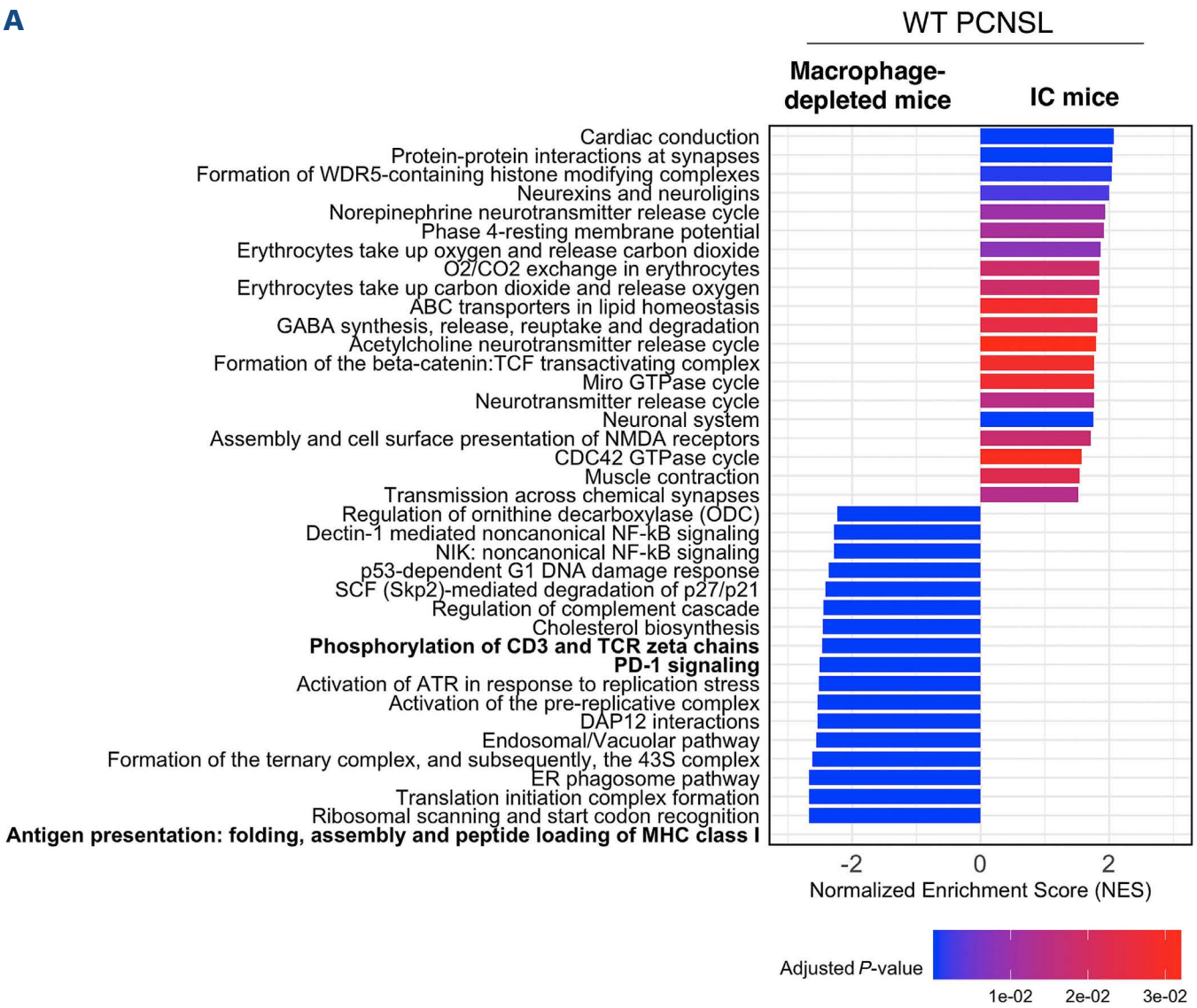
These findings emphasize the important role of MHC-I in immune-mediated tumor control and reveal distinct transcriptional responses to PD1 blockade which are dependent on MHC-I expression in the TME.

Discussion

Our research highlights the dynamic interplay between malignant cells, macrophages, and T cells within the TME of primary CNS lymphoma. We demonstrate that macrophages play a crucial role in the pathogenesis of primary CNS lymphoma as well as in the anti-tumor response to immune checkpoint blockade.

In many solid tumors, tumor-associated macrophages frequently adopt an immunosuppressive M2-like phenotype that facilitates tumor progression and diminishes the efficacy of immune checkpoint blockade. To counteract this, agents such as pexidartinib are being investigated for their capacity to deplete or reprogram these macrophages, with promising results in shifting them toward a pro-inflammatory, anti-tumoral M1-like phenotype.[31] This strategy has also shown encouraging effects in preclinical lymphoma models, including DLBCL, follicular lymphoma, and Burkitt lymphoma, by enhancing macrophage-mediated anti-tumor responses.[32] However, Gao *et al*. demonstrated that CSF1R inhibition using pexidartinib after PCNSL induction in mice paradoxically accelerated tumor progression.[17] This divergence likely reflects the distinct immunologic landscape of the CNS, where infiltrating macrophages and resident microglia exhibit context-dependent functions. In our experimental model, depletion of these myeloid populations prior to tumor implantation similarly resulted in a more aggressive disease phenotype. Here, we confirmed that macrophages and microglia serve as anti-tumoral effectors in PCNSL. Microglial cells, in particular, may act as the first immune cells to engage tumor cells in the CNS, shaping the subsequent immune landscape and influencing the timing and extent of macrophage and T-cell infiltration. Consistent with our findings, several studies have demonstrated that macrophages robustly infiltrate the brain in human PCNSL and constitute a major component of the tumor microenvironment.[15-18] Komohara *et al*.[15] analyzed tumor samples from 43 PCNSL patients and showed by IHC that $CD86^+$ macrophages constitute a predominant population within the tumor microenvironment. Nam *et al*.[16] examined 104 PCNSL specimens and observed significant infiltration of macrophages, with higher $CD86^+$ cell densities correlating with improved progression-free survival (PFS). Gao *et al*.[17] analyzed 62 diagnostic specimens from IC PCNSL patients and found that lower density and smaller size of $CD68^+$ TAM significantly correlated with shorter overall survival (OS). Interestingly, strong TAP1 expression independently predicted improved PFS, supporting the protecting role of tumor-associated macrophages against PCNSL progression. Moreover, Pollari *et al*.[18] further characterized macrophage subpopulations and found that a high pro-

A



B

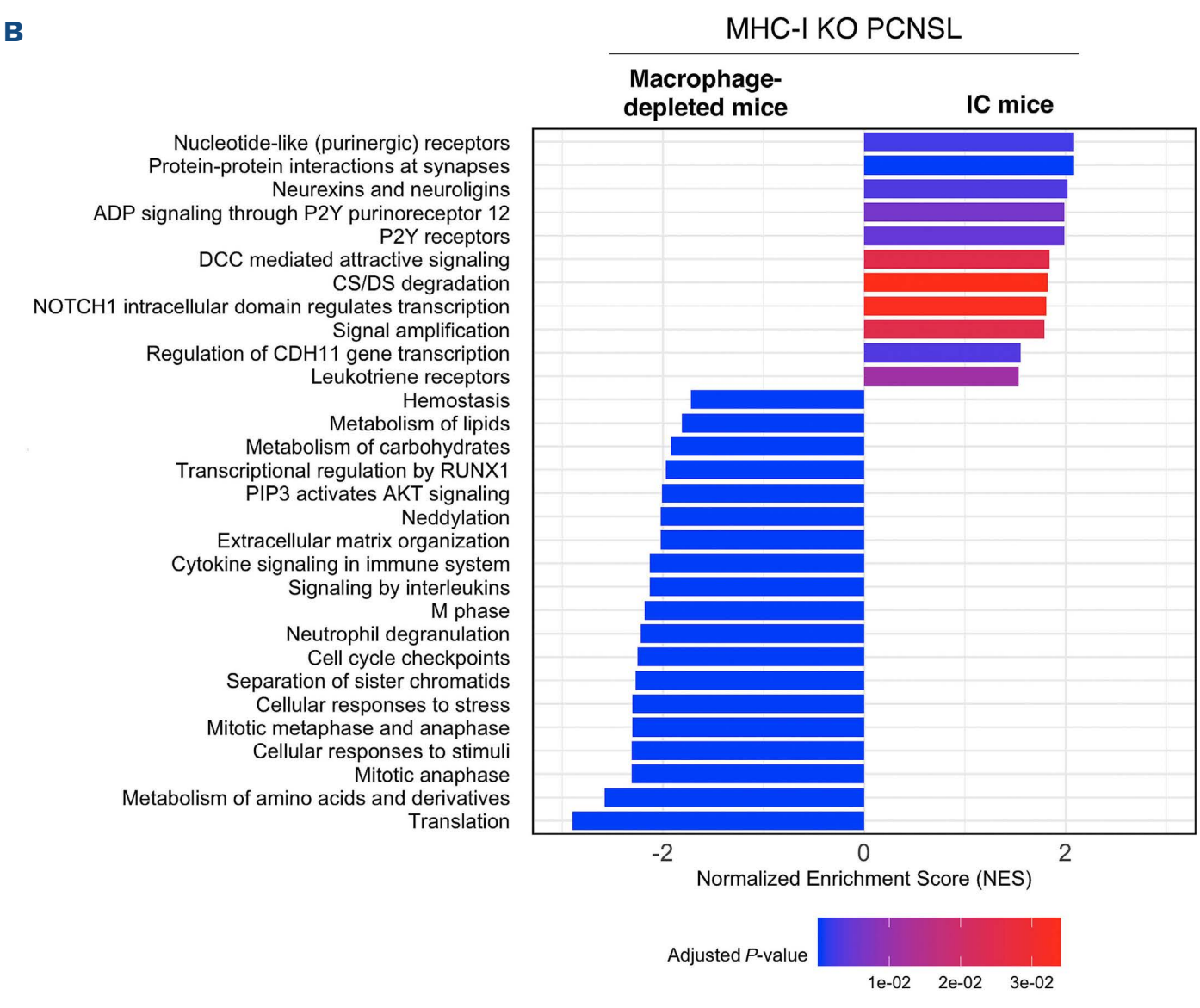


Figure 8. Pathway enrichment analysis comparisons between groups. (A and B) Bar plots representing normalized enrichment scores (NES) from Gene Set Enrichment Analysis (GSEA) using the Reactome database, comparing immunocompetent (IC) mice to macrophage-depleted mice bearing either wild-type (WT) primary central nervous system lymphoma (PCNSL) (A) or MHC-I knockout (KO) PCNSL (B). The y-axis displays the enriched pathways, while the x-axis shows the NES values. Pathways are colored according to their statistical significance, indicating adjusted *P* values.

portion of PD-L1⁺CD68⁺ macrophages was associated with improved OS and disease-specific survival.

In our macrophage-competent PCNSL mouse models, PD1 blockade was significantly more effective than in MD models, highlighting a crucial and non-redundant role for macrophages and microglia in the response to anti-PD1 therapy, besides the expected role of cytotoxic T lymphocytes. This effect was further enhanced in tumors retaining intact MHC-I expression. Together, our findings suggest that effective T-cell activation in PCNSL depends on the coordinated involvement of both macrophages and microglia, emphasizing the importance of antigen cross-presentation in linking innate and adaptive anti-tumor immunity within the CNS microenvironment. Preclinical and clinical studies provide a strong biological rationale for targeting PD1 in PCNSL.[12,25] Early-phase clinical trials have shown promising initial responses in relapsed or refractory PCNSL patients;[12] however, these responses are often short, with most patients eventually experiencing relapse. A major factor limiting the durability of PD1 blockade is the loss of MHC-I expression in tumor cells, as also demonstrated in our findings. Consistent with this, few studies have corroborated the loss of HLA class I expression in patients, associated with outcome.[8-10] Riemersma *et al.*[10] reported total loss of HLA-A expression in 60% of extranodal lymphomas (including primary CNS and testicular lymphomas, both considered immune-privileged sites) compared with only 10% in nodal cases. Interestingly, Geng *et al.*[7] correlated genomic lesions at the HLA class I locus with clinical outcomes in PCNSL. In their cohort of 78 patients, 6p CN-LOH/6p21.3 homozygous deletions affecting HLA-A, -B, and -C in 16 cases defined a high-risk subgroup with significantly shorter PFS and OS. Furthermore, Alame *et al.*[9] observed that lower HLA gene expression is associated with an immune-poor TME correlated with bad prognosis in patients. This establishes impaired HLA class I-mediated antigen presentation as a major prognostic factor clinically associated with poorer outcomes in PCNSL patients.

While loss of HLA class I expression in lymphomas arising in immune-privileged sites such as PCNSL may appear to be a redundant immune evasion benefit given the low baseline immune surveillance in these compartments, it remains to be investigated whether such genomic alterations represent a positive selection feature. These mutations might allow tumor cells to proliferate in these sites without triggering any unwanted immune response, potentially facilitating tumor growth through subtle modulation of local immunity rather than overt immune evasion.

A limitation of our study is the use of the intracerebral A20 model. Although this model is robust and widely employed to investigate pathogenesis and evaluate novel therapeutic strategies in PCNSL, it does not fully recapitulate the natural clinical origin or B-cell tropism observed in human disease. Accordingly, caution is warranted when extrapolating these findings to patients. Despite these limitations, the model remains a valuable tool for dissecting CNS-specific immune mechanisms within a controlled experimental setting.

Collectively, therapeutic strategies must go beyond T-cell reinvigoration and include targeting of the macrophage-microglia compartment. Such combinatorial approaches could bypass the need for MHC-I-dependent immune recognition and address the immune resistance observed in PCNSL.

Disclosures

KW reports patents/royalties from Stanford University, Whitehead Institute, Forty Seven, Gilead Sciences, ALX Oncology, DEM Biopharma, Inograft, and Bitterroot Bio; is co-founder, past or present scientific advisory board member, and equity holder in ALX Oncology, DEM Biopharma, and Solu Therapeutics; and holds stock in Ginkgo Bioworks, and Inograft. FB has received honoraria from Roche, Novartis, AstraZeneca, Lilly, BMS GmbH & Co KG, Merck, Johnson & Johnson/Janssen, BeiGene, Advantage Pharmaceuticals, ASCEND Therapeutics, and AbbVie; has served on advisory boards or as a consultant for AstraZeneca, Roche/Genentech, Janssen-Cilag, Lilly, AbbVie, Kite (a Gilead company), BeiGene, and Novartis; has participated in speakers' bureaus for AbbVie, Janssen, Roche, AstraZeneca, Merck, Bristol Myers Squibb/Celgene, Kite/Gilead, and Johnson & Johnson/Janssen; has received research funding from Janssen, Gilead, Genentech, and AstraZeneca; and has received travel support from AstraZeneca, BeiGene, Johnson & Johnson/Janssen, and AbbVie. MC reports honoraria from Janssen, Lilly, and AstraZeneca; and research funding from Karyopharm, Janssen, AstraZeneca, and Genetech. All the other authors have no conflicts of interest to disclose.

Contributions

CPG designed and performed mouse experiments, is responsible for cell line maintenance, data analysis, and performed assays, wrote the first draft and revised the manuscript. JC designed and performed mouse experiments. MC is responsible for experimental design, oversight and funding acquisition, wrote the first draft and revised the manuscript. DMG, PFG, CH and GP are responsible for cell line maintenance, data analysis, and performed assays. KW and FB are responsible for experimental design, oversight and funding acquisition. All authors reviewed and edited the manuscript, and are responsible for its contents.

Acknowledgments

We thank the State Agency for Research (Agencia Estatal de Investigación) for Severo Ochoa Center of Excellence funding (CEX2020-001024-S/AEI/10.13039/501100011033), the Cellex Foundation for research facilities/equipment, and the CERCA Program (Generalitat de Catalunya). We also thank Guillem Colell (VHIO) for in vivo support and Athanasios Ploumakis (Spatial Technologies Unit, Precision RNA Medicine Core, Harvard Medical School) for multiplexed IF assistance.

Funding

This work was supported by research funding from the Instituto de Salud Carlos III, Fondo de Investigaciones Sanitarias (PI21/01190 and PI25/00775 MC; PI20/01274 and PI24/00529; to FB), Fundació la Marató de TV3 (201905-30-31; to FB), and Asociación Española Contra el Cáncer (LABAE18014CRES; to MC). All Spanish funding was co-sponsored by the European Union FEDER program "Una manera de hacer Europa". Additional support came from Valhalla Foundation, AACR-AstraZeneca Career Development Award for Physician-Scientists in Honor of José Baselga, and an anonymous grant, Richard Reisman in honor of Jane Reisman and Lilian Reisman, Research Foundation for the Treatment of Ovarian Cancer, ALK Positive Lung Cancer Foundation, Torrey Coast Foundation, Department of Defense grant W81XWH2210141, and National Cancer Institute grant R01CA279259 (all to KW). DM-G holds a contract from Agència de Gestió d'Ajuts Universitaris i de Recerca (AGAUR) (2022FI_B 00092).

Data-sharing statement

The data generated in this study are available within the article and in its Online Supplementary Appendix.

References

1. Lv C, Wang J, Zhou M, et al. Primary central nervous system lymphoma in the United States, 1975-2017. Ther Adv Hematol. 2022;13:20406207211066166.
2. Mo SS, Cleveland J, Rubenstein JL. Primary CNS lymphoma: update on molecular pathogenesis and therapy. Leuk Lymphoma. 2023;64(1):57-65.
3. Alaggio R, Amador C, Anagnostopoulos I, et al. The 5th edition of the World Health Organization Classification of Haematolymphoid Tumours: Lymphoid Neoplasms. Leukemia. 2022;36(7):1720-1748.
4. Schmitz R, Wright GW, Huang DW, et al. Genetics and pathogenesis of diffuse large B cell lymphoma. N Engl J Med. 2018;378(15):1396-1407.
5. Chapuy B, Stewart C, Dunford AJ, et al. Molecular subtypes of diffuse large B cell lymphoma are associated with distinct pathogenic mechanisms and outcomes. Nat Med. 2018;24(5):679-690.
6. Bordon Y. Guardians of immune privilege. Nat Rev Immunol. 2025;25(1):1.
7. Geng H, Mo SS, Chen L, et al. Identification of genomic biomarkers of disease progression and survival in primary CNS lymphoma. Blood Adv. 2024;9(5):1117-1131.
8. Minderman M, Amir A, Kraan W, et al. Immune evasion in primary testicular and central nervous system lymphomas: HLA loss rather than 9p24.1/PD-L1/PD-L2 alterations. Blood Adv. 2021;5(7):1873-1883.
9. Alame M, Cornillot E, Cacheux V, et al. The immune contexture of primary central nervous system diffuse large B cell lymphoma associates with patient survival and specific cell signaling. Theranostics. 2021;11(8):3565-3579.
10. Riemersma SA, Jordanova ES, Schop RFJ, et al. Extensive genetic alterations of the HLA region, including homozygous deletions of HLA class II genes in B cell lymphomas arising in immune-privileged sites. Blood. 2000;96(10):3569-3577.
11. Chapuy B, Roemer MGM, Stewart C, et al. Targetable genetic features of primary testicular and primary central nervous system lymphomas. Blood. 2016;127(7):869-881.
12. Nayak L, Iwamoto FM, LaCasce A, et al. PD1 blockade with nivolumab in relapsed/refractory primary central nervous system and testicular lymphoma. Blood. 2017;129(23):3071-3073.
13. Hoang-Xuan K, Houot R, Soussain C, et al. First results of the Acsé pembrolizumab phase II in the primary CNS lymphoma (PCNSL) cohort. Blood. 2020;136(Supplement 1):15-16.
14. Heming M, Haessner S, Wolbert J, et al. Intratumor heterogeneity and T cell exhaustion in primary CNS lymphoma. Genome Med. 2022;14(1):109.
15. Komohara Y, Horlad H, Ohnishi K, et al. M2 macrophage/microglial cells induce activation of Stat3 in primary central nervous system lymphoma. J Clin Exp Hematopathol. 2011;51(2):93-99.
16. Nam SJ, Kim S, Kwon D, et al. Prognostic implications of tumor-infiltrating macrophages, M2 macrophages, regulatory T cells, and indoleamine 2,3-dioxygenase-positive cells in primary diffuse large B cell lymphoma of the central nervous system. Oncoimmunology. 2018;7(7):e1442164.
17. Gao H-X, Fraser E, Merlini M, et al. Regulation of CNS lymphoma progression by the myeloid microenvironment. Blood. 2021;138(Supplement 1):448.
18. Pollari M, Brück O, Pellinen T, et al. PD-L1+ tumor-associated macrophages and PD1+ tumor-infiltrating lymphocytes predict survival in primary testicular lymphoma. Haematologica. 2018;103(11):1908-1914.
19. Shi L, Chen S, Yang L, Li Y. The role of PD1 and PD-L1 in T cell immune suppression in patients with hematological malignancies. J Hematol Oncol. 2013;6(1):74.
20. Zuazo M, Gato-Cañas M, Llorente N, et al. Molecular mechanisms of programmed cell death-1 dependent T cell suppression: relevance for immunotherapy. Ann Transl Med. 2017;5(19):385.
21. Gordon SR, Maute RL, Dulken BW, et al. PD1 expression by tumour-associated macrophages inhibits phagocytosis and tumour immunity. Nature. 2017;545(7655):495-499.
22. Barkal AA, Weiskopf K, Kao KS, et al. Engagement of MHC class I by the inhibitory receptor LILRB1 suppresses macrophages and is a target of cancer immunotherapy. Nat Immunol. 2018;19(1):76-84.
23. Nieto P, Klinsing S, Caratù G, et al. Decoding the immune response in leptomeningeal disease through single-cell sequencing of cerebrospinal fluid. bioRxiv. Accessed Jan 27, 2025. https://doi.org/10.1101/2025.01.27.634744 [preprint, not peer-reviewed].
24. Jiménez I, Carabia J, Bobillo S, et al. Repolarization of tumor infiltrating macrophages and increased survival in mouse primary CNS lymphomas after XPO1 and BTK inhibition. J Neurooncol. 2020;149(1):13-25.
25. Qiu Y, Li Z, Pouzoulet F, et al. Immune checkpoint inhibition by anti-PDCD1 (anti-PD1) monoclonal antibody has significant therapeutic activity against central nervous system lymphoma in an immunocompetent preclinical model. Br J Hematol.

2018;180(2):278-281.
26. Donnou S, Galand C, Daussy C, et al. Immune adaptive microenvironment profiles in intracerebral and intrasplenic lymphomas share common characteristics. Clin Exp Immunol. 2011;165(3):329-337.
27. Zhang S, Shen J, Li D, Cheng Y. Strategies in the delivery of Cas9 ribonucleoprotein for CRISPR/Cas9 genome editing. Theranostics. 2021;11(2):614-648.
28. Pennartz S, Reiss S, Biloune R, Hasselmann D, Bosio A. Generation of single-cell suspensions from mouse neural tissue. J Vis Exp. 2009;29:1267.
29. Mantel I, Sadiq BA, Blander JM. Spotlight on TAP and its vital role in antigen presentation and cross-presentation. Mol Immunol. 2022;142:105-119.
30. Majid U, Bergsland CH, Sveen A, et al. The prognostic effect of tumor-associated macrophages in stage I-III colorectal cancer depends on T cell infiltration. Cell Oncol (Dordr). 2024;47(4):1267-1276.
31. Patnaik A, Eisenberg PD, Sachdev JC, et al. Phase 1/2a study of double immune suppression blockade by combining a CSF1R inhibitor (Pexidartinib/PLX3397) with an anti PD1 antibody (Pembrolizumab) to treat advanced, solid tumors. J Clin Oncol. 2016;34(15_suppl):TPS11618.
32. Valero JG, Matas-Céspedes A, Arenas F, et al. The receptor of the colony-stimulating factor-1 (CSF-1R) is a novel prognostic factor and therapeutic target in follicular lymphoma. Leukemia. 2021;35(9):2635-2649.